ELSEVIER

International Journal of Mass Spectrometry 182/183 (1999) 99–120

International Journal of Mass Spectrometry

Reactions of $Cu^+(^1S$ and $^3D)$ with O_2, CO, CO_2, N_2, NO, N_2O, and NO_2 studied by guided ion beam mass spectrometry

M.T. Rodgers[a], Ben Walker[b,1], P.B. Armentrout[b,*]

Department of Chemistry, Wayne State University, Detroit, MI 48202, USA
Department of Chemistry, University of Utah, Salt Lake City, UT 84112, USA

Received 15 July 1998; accepted 30 August 1998

Abstract

Reactions of $Cu^+(^1S$ and $^3D)$ with O_2, CO, CO_2, N_2, NO, N_2O, and NO_2 are studied using guided ion beam mass spectrometry. Cross sections as a function of kinetic energy are measured for each system to over 17 eV. In all cases, the observed reactions of $Cu^+(^1S)$ are endothermic. Because of the closed shell character of ground state Cu^+ $(^1S, 3d^{10})$, most of these systems exhibit cross sections with onsets and peaks at much higher energies than expected from the known thermochemistry. Such behavior indicates that the reactions occur on relatively repulsive potential energy surfaces and by impulsive processes. Reliable thermodynamic information is obtained primarily from the NO_2 system where an analysis of the kinetic energy dependence of the reaction cross sections is used to obtain $D_0(Cu^+–O) = 1.35 \pm 0.12$ eV and $D_0(Cu–O) = 2.94 \pm 0.12$ eV. Although speculative, the threshold for an excited state product asymptote in the N_2O system also allows the derivation of $D_0(Cu^+–N_2) = 0.92 \pm 0.31$ eV. Reactions of the $Cu^+(^3D, 4s^1\ 3d^9)$ excited state are generally more efficient than those of the ground state and are exothermic in several cases. (Int J Mass Spectrom 182/183 (1999) 99–120) © 1999 Elsevier Science B.V.

Keywords: Copper ions; Atmospheric gases; Bond energies; Impulsive dynamics; Guided ion beams

1. Introduction

Compared with its open shell transition metal neighbors, copper monocations are relatively unreactive with many nonpolar molecules and small molecules [1–8]. However, given sufficient energy [2–7] or with larger hydrocarbons [9], Cu^+ ions react by mechanisms similar to other later transition metal ions but with an enhanced probability of abstracting H^- and R^- groups to form the closed shell CuH and CuR molecules. Pioneering work by Freiser and co-workers, as well as a number of later studies by other investigators, find that Cu^+ is much more reactive with polar molecules, inducing a number of dissociative attachment reactions at thermal energies [10–22]. One of the driving forces for this enhanced reactivity with polar molecules is that Cu^+ is a very effective Lewis acid, strongly binding molecules with accessible pairs of electrons [23–33]. Indeed, bond energies of Lewis bases to Cu^+ are relatively strong compared with other transition metal ions because copper lies to

* Corresponding author.
[1]Present address: Sentrol, 12345 Leveton Dr., Tualatin, OR 97062.

In memory of Ben S. Freiser, a good friend and colleague, and in thanks for his many contributions to gas-phase ion chemistry.

PII S1387-3806(98)14228-8

Table 1
Thermodynamic and pairwise dissociation energies for reaction of $Cu^+(^1S, {}^3D^*)$

Reactant (BC)	Products (AB + C)	Mass factor [a]	D_0(BC) eV [b]	D_0^*(BC) eV [c]	D_{0P}(BC) eV [d]	D_{0P}^*(BC) eV [e]
O_2	$CuO^+ + O$	1.663	5.116	2.31	8.5	3.8
CO	$CuO^+ + C$	1.519	11.108	8.30	16.9	12.6
	$CuC^+ + O$	1.923	11.108	8.30	21.4	16.0
CO_2	$CuO^+ + CO$	2.030	5.453	2.64	11.1	5.4
	$CuO^+ + C + O$	2.030	16.561	13.75	33.6	27.9
	$CuCO^+ + O$	1.336	5.453	2.64	7.3	3.5
N_2	$CuN^+ + N$	1.692	9.759	6.95	16.5	11.8
NO	$CuO^+ + N$	1.593	6.507	3.70	10.4	5.9
	$CuN^+ + O$	1.774	6.507	3.70	11.5	6.6
N_2O	$CuO^+ + N_2$	2.030	1.672	< 0	3.4	< 0
	$CuO^+ + N + N$	2.030	11.431	8.62	23.2	17.5
	$CuN_2^+ + O(^3P)$	1.336	1.672	< 0	2.2	< 0
	$CuN_2^+ + O(^1D)$	1.336	3.640	0.83	4.9	< 0
	$CuN^+ + NO$	2.261	4.924	2.11	11.1	4.8
	$CuN^+ + NO$	2.261	8.431	5.62	19.1	12.7
NO_2	$CuO^+ + NO$	2.083	3.116	0.31	6.5	0.6
	$CuO^+ + N + O$	2.083	9.623	6.81	20.1	14.2
	$CuNO^+ + O$	1.308	3.116	0.31	4.1	0.4

[a] The mass factor in Eq. (1): $(A + B)(B + C)/B(A + B + C)$.
[b] Chase et al. [44].
[c] $D_0^*(\mathrm{BC}) = D_0(\mathrm{BC}) - E^*(^3D)$.
[d] $D_{0P}(\mathrm{BC}) = D_0(\mathrm{BC}) \times (A + B)(B + C)/B(A + B + C)$.
[e] $D_{0P}^*(\mathrm{BC}) = D_0^*(\mathrm{BC}) \times (A + B)(B + C)/B(A + B + C)$.

the right of the transition series and is therefore relatively small.

In this work, we investigate the reactions of atomic copper ions with several atmospheric gases: O_2, CO, CO_2, N_2, NO, N_2O, and NO_2. Except for the O_2 and N_2O systems [5,34], none of these reaction systems has been investigated previously although some of the unusual product ions observed in this work have been reported [35–37]. In the present work, the ion source conditions can be varied such that reactions of both ground state $Cu^+(^1S, 3d^{10})$ and first excited state $Cu^+(^3D, 4s^13d^9)$ can be investigated. The latter state lies 2.81 eV = $E^*(^3D)$ above the ground state [38]. (This excitation energy is the average of the 3, 2, and 1 spin–orbit levels weighted by the degeneracies, i.e. the distribution expected at an infinite temperature.)

In previous work [5], it has been suggested that the closed shell nature of ground state $Cu^+(^1S, 3d^{10})$ can lead to impulsive reaction dynamics. In a completely impulsive reaction limit, the copper ion interacts with only a single atom of the neutral reagent such that the effective energy available for reaction differs strongly from the center-of-mass (CM) energy. In this pairwise interaction limit, the effective energy of the Cu^+-molecule collision is determined by the relative energy between the incoming Cu^+ ion (having mass A) and the atom first struck (with mass B), rather than between Cu^+ and the entire BC molecule. This pairwise energy is related to the CM energy by Eq. (1).

$$E(\mathrm{CM}) = E(\mathrm{pair}) \times (A + B)(B + C)/B(A + B + C) \quad (1)$$

In the limit that $A \gg B$ and C, it can be seen that the mass factor in Eq. (1) reduces to $(B + C)/B$. This formula shows that E(pair) is less than E(CM). Hence, reactions occurring in the impulsive, pairwise limit require substantially higher CM energies than those thermodynamically permitted.

Some of the consequences of this for the systems of interest here are summarized in Table 1. Here, the

mass factors of Eq. (1) are listed along with the bond energies of the reactant BC molecules. Ordinarily, cross sections for reaction of $A^+ + BC \rightarrow AB^+ + C$ reach a maximum at $D_0(BC)$ because at this energy the AB^+ product can begin to dissociate to $A^+ + B$. However, if this reaction occurs impulsively, then the onset for this dissociation process is shifted to higher energies according to Eq. (1), i.e. E(pair) must equal $D_0(BC)$. If the reaction is completely impulsive, the maximum in the cross section will occur at center-of-mass energies corresponding to the values of D_{0P} listed in Table 1. Corresponding dissociation energies in the thermodynamic and impulsive limits for reaction of $Cu^+(^3D)$ are also given in this table. Clearly the onset for formation of AB^+ can also be shifted. We will find that the predictions of Table 1 are remarkably useful in the present study.

2. Experimental

2.1. General procedures

Cross sections for reaction of $Cu^+(^1S$ and $^3D)$ with O_2, CO, CO_2, N_2, NO, N_2O, and NO_2 are studied using a guided ion beam mass spectrometer that has been described in detail elsewhere [39,40]. The copper ions are generated as described below. The ions are extracted from the source, accelerated, and focused into a magnetic sector momentum analyzer for mass analysis. Mass-selected ions are decelerated to a desired kinetic energy and focused into an octopole ion guide, which traps the ions in the radial direction [41]. The octopole passes through a static gas cell containing the neutral reactant. Low gas pressures in the cell (typically 0.1–0.2 mTorr) are used to ensure that multiple ion-molecule collisions are improbable. All cross sections presented here are invariant to changes in the neutral pressure (except as noted in one case) indicating they are the result of single bimolecular encounters. Product and unreacted Cu^+ ions drift to the end of the octopole where they are focused into a quadrupole mass filter for mass analysis and subsequently detected with a secondary electron scintillation detector and standard pulse counting techniques. Ion intensities are then converted to absolute cross sections as previously described [39]. Absolute uncertainties in cross sections are estimated to be ± 20% unless otherwise specified.

Ion kinetic energies in the laboratory frame, E(lab), are converted to energies in the center-of-mass frame, E(CM), using the formula, $E(\mathrm{CM}) = E(\mathrm{lab})\, m/(m + M)$, where m and M are the neutral and ionic reactant masses, respectively. All energies reported below are in the CM frame unless otherwise noted. The absolute zero and distribution of the ion kinetic energies are determined using the octopole ion guide as a retarding potential analyzer as previously described [39]. The distribution of reactant ion kinetic energies is nearly Gaussian with a FWHM of ~ 0.40 eV (lab) for these experiments. The uncertainty in the absolute energy scale is ± 0.05 eV (lab).

The reactions in this work are studied to fairly high kinetic energies. In order to ensure that product ions are collected efficiently, this requires a relatively high dc bias voltage on the quadrupole mass filter used to analyze the product ions. This, in turn, reduces the mass resolution of the mass spectrometer such that product ions separated by only a few mass units (e.g. CuC^+, CuN^+, and CuO^+) are not completely resolved. If the mass resolution is increased to alleviate this problem, the collection efficiency again suffers. Hence, we collect data under both low and high resolution conditions. The high resolution data allow a separation of the product ions and efficient collection at lower kinetic energies while the low resolution data provides efficient collection over the entire energy range, but with substantial mass overlap for closely spaced masses. This latter data is easily corrected for the mass overlap as the energy dependence of the products is generally distinct. The accuracy of this correction is then verified by the high resolution data. The results illustrated below have been corrected in this fashion when necessary.

The various gases used in these experiments were used as received. However, problems were encountered using NO and NO_2 as it is extremely difficult to keep nitrogen oxides contaminant free. NO readily reacts with O_2 to form NO_2. The nitrogen oxides react with one another to form N_2O_3 and N_2O_4 and with

water to form various acids, e.g. HNO_2 and HNO_3. The acids can then attack residual material on the gas inlet surfaces to produce other species. Trace amounts of these contaminants were apparently present in the work reported here, but reactions with these unidentifiable species can be easily ascertained on the basis of known thermodynamics. Moreover, cross section features attributable to the contaminants increased between subsequent data sets over the course of a day, while those associated with NO and NO_2 did not. As these contaminants are very difficult to remove entirely and they do not affect the key energy regions of the cross sections examined here, attempts to acquire additional data free from contamination were deemed unnecessary.

2.2. Ion source

Cu^+ ions are generated in a 1 m long flow tube [40] operating at a pressure of 0.5–0.7 Torr with a helium flow rate of 4000–7000 sccm. A dc discharge at a voltage of 0.8–1.4 kV is used to ionize Ar. The Ar^+ ions are accelerated into a cathode made of copper. This produces Cu^+ ions that are swept down the flow tube and undergo $> 10^5$ collisions with the He and Ar bath gases. Under these conditions, most excited states of Cu^+ are quenched to their ground state by these collisions. Complete quenching of the excited electronic states is achieved by introducing a small amount of nitric oxide ($\sim$ 3–4 mTorr) to the flow [42]. This is demonstrated below.

2.3. Thermochemical analysis

The threshold regions of the reaction cross sections are modeled using Eq. (2),

$$\sigma(E) = \sigma_0 \sum_i g_i(E + E_i + E_{\text{int}} - E_0)^n/E \qquad (2)$$

which involves an explicit sum of the contributions of individual electronic states of the Cu^+ reactant, denoted by i, with energies E_i and populations g_i. In Eq. (2), E is the relative kinetic energy, σ_0 is an energy independent scaling factor, and E_0 is the 0 K threshold for reaction of ground electronic, vibrational, and rotational state reactants. E_{int} is the internal energy of the neutral reactant including rotations and vibrations. The rotational energies are $k_BT = 0.026$ eV for O_2, CO, CO_2, N_2, NO, and N_2O and $3k_BT/2 = 0.039$ eV for NO_2 at 305 K, the nominal temperature of the octopole. The average reactant vibrational energies are less than 1 meV for O_2, CO, N_2, and NO, 7.4 meV for CO_2, 9.5 meV for N_2O, and 3.0 meV for NO_2 [43,44]. Before comparison with the data, Eq. (2) is convoluted with the kinetic energy distributions of the ion and neutral reactants [39]. The σ_0, n, and E_0 parameters are then optimized using a nonlinear least squares analysis to give the best reproduction of the data. Error limits for E_0 are calculated from the range of threshold values for different data sets obtained with a range of acceptable n values and the uncertainty in the absolute energy scale.

At high energies, the cross sections decline because the product ions have sufficient energy to dissociate. In this high energy region, the data can be modeled by modifying Eq. (2) to include the dissociation probability according to a statistical model discussed elsewhere [45]. This dissociation probability is controlled by two parameters: E_D, which is the energy at which product ions begin decomposing, and p, which is an adjustable parameter similar to n in Eq. (2). In this study, the values of p and E_D are allowed to vary (although p can only hold integral values). Use of this high-energy model does not significantly alter the analysis of the threshold regions.

3. Results

3.1. $Cu^+ + O_2$

Copper cations react with molecular oxygen to form one ionic product, CuO^+. The reaction is endothermic and corresponds to reaction (3).

$$Cu^+ + O_2 \rightarrow CuO^+ + O \qquad (3)$$

The energy dependence of the cross section for this process with Cu^+ is shown in Fig. 1. When NO is added to the flow tube, the results obtained are in excellent agreement (both energy dependence and

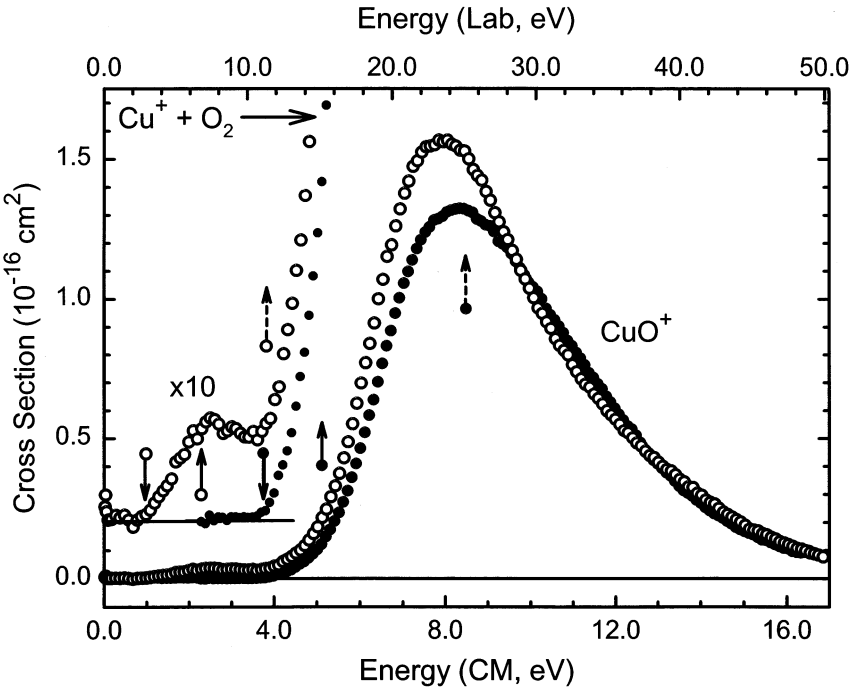

Fig. 1. Variation of the cross sections for reaction of Cu^+ with O_2 as a function of translational energy in the center-of-mass frame (lower scale) and laboratory frame (upper scale). Data are shown for Cu^+ ions formed by dc discharge with (●) and without (○) the addition of NO to the flow tube. The inset shows the data on an expanded vertical scale (× 10) and offset from zero. Downward arrows indicate the thermodynamic thresholds for CuO^+ formation from $Cu^+(^1S)$ and $Cu^+(^3D)$ at 3.77 and 0.96 eV, respectively. Upward arrows show the thermodynamic thresholds for atomization, reaction (4), for reaction with Cu^+ (^1S) and Cu^+ (^3D) at 5.12 and 2.31 eV, respectively. Dashed upward arrows show the thresholds for atomization on an impulsive energy scale for reaction with Cu^+ (^1S) and Cu^+ (^3D) at 8.5 and 3.8 eV, respectively. In this and all figures, solid arrows indicate thermodynamic quantities while dashed arrows indicate impulsive energies. Arrows are marked by the symbol to which they correspond. Upward arrows indicate dissociation processes for which energies are taken from Table 1. Downward arrows indicate reaction thresholds for which energies are taken from Table 4.

magnitude) with previous results obtained by generating Cu^+ using surface ionization, which produces 100% $Cu^+(^1S)$ [5]. Thus, the NO acts to efficiently quench excited state Cu^+ ions formed in the dc discharge source, resulting in a Cu^+ beam that is pure ground state ^1S ions. The cross section rises slowly from an apparent threshold below 4 eV and peaks at ~ 8 eV. As noted previously [5], this is unusual behavior as the cross sections for the analogous reactions with other transition metal cations peak close to the thermodynamic threshold for dissociation of the MO^+ product. This is the overall reaction (4), which has an onset equal to $D_0(O_2)$, Table 1.

$$M^+ + O_2 \rightarrow M^+ + O + O \quad (4)$$

The observation that the peak of the CuO^+ cross section occurs at higher energies indicates that the reaction dynamics favor placing excess energy in translation rather than in internal energy of the diatomic product. We have previously suggested that this indicates impulsive reaction dynamics [5]. Indeed, the threshold for reaction (4) on the pairwise energy scale, i.e. E(CM) when E(pair) = $D_0(O_2)$, is 8.5 eV, Table 1. This prediction is in good agreement with the observed peak of the CuO^+ cross section (Fig. 1).

Without NO cooling gas in the flow tube, a small low energy feature in the CuO^+ cross section is observed. This is obviously attributable to the reaction of excited state Cu^+ with O_2. The apparent threshold

occurs at ~ 1 eV, approximately 3 eV below the threshold for reaction of $Cu^+(^1S)$. The reaction cross section rises from threshold more rapidly than for ground state Cu^+ and the peak of the reaction cross section occurs at ~ 2.3 eV, 2.8 eV below the thermodynamic threshold for reaction (4). These energetics clearly indicate that the $^3D(4s^13d^9)$ first excited state of Cu^+ lying 2.81 eV = $E^*(^3D)$ above the ground state is responsible for this low energy feature. A similar low energy feature was previously observed in the reaction of Cu^+ ions produced by electron ionization (EI) of $Cu(CH_3CO_2)$ [5]. However, the apparent threshold and peak of the reaction cross section occurred at lower energies in the EI data. There, it was concluded that the Cu^+ beam produced by EI also contains Cu^+ in its ^1D state at 3.26 eV [5]. In addition, the magnitude of this low energy feature is larger by a factor of ~ 2 in the EI data, probably indicating that the excited state population is larger for the EI produced ions than for the dc discharge source.

3.2. $Cu^+ + CO$

The reaction of Cu^+ with CO forms two products, CuO^+ and CuC^+, in processes (5) and (6). Cross sections for $Cu^+(^1S)$ are shown in Fig. 2(a). No reactivity is observed below 10 eV.

$$Cu^+ + CO \rightarrow CuO^+ + C \quad (5)$$

$$\rightarrow CuC^+ + O \quad (6)$$

Both reaction pathways exhibit thresholds in excess of D_0(CO), Table 1. This means that formation of CuO^+ and CuC^+ does not even begin until above the energy where they can dissociate. As a consequence, these thresholds have no simple thermodynamic meaning. Formation of stable diatomic products above D_0(CO) can only occur if substantial amounts of energy are placed in translation or electronic excitation of the products, suggesting that impulsive reactivity may control this reaction. In an impulsive limit, dissociation of the CuC^+ and CuO^+ products is predicted to be delayed until 21.4 and 16.9 eV, respectively (Table 1). It can be seen in Fig. 2(a) that the peak of the CuO^+ cross section occurs close to 17 eV, in agreement with this prediction. Likewise, the CuC^+ cross section plateaus and then decreases more rapidly at about 22 eV. Certainly, the distinct high energy behavior of the two products is qualitatively described by the impulsive model and contrasts with the thermodynamic expectation that both peaks should occur at about 11.1 eV = D_0(CO). In contrast, this latter expectation is fulfilled in the reactions of early transition metal ions reacting with CO [46,47].

For the CO system, results obtained without NO cooling gas in the flow tube are shown in Fig. 2(b). As for the O_2 reaction, the results are dominated by the ground state reactivity. However, low energy features are now seen in both the CuC^+ and CuO^+ cross sections and these can again be attributed to reaction of $Cu^+(^3D)$. Above about 17 eV, the magnitudes of these cross sections begin to differ from those shown in Fig. 2(a). This is an experimental artifact associated with differing experimental conditions used to collect the data.

3.3. $Cu^+ + CO_2$

The reaction of Cu^+ with CO_2 produces two products, CuO^+ and $CuCO^+$, in reactions (7) and (8). Cross sections for these processes are shown in Fig. 3.

$$Cu^+ + CO_2 \rightarrow CuO^+ + CO \quad (7)$$

$$\rightarrow CuCO^+ + O \quad (8)$$

Both products correspond to cleavage of the OC–O bond. The major reaction pathway observed for this system leads to the formation of CuO^+. The CuO^+ cross section rises from an apparent threshold near 4 eV before reaching a maximum at about 10 eV. Rather than peaking near D_0(OC–O), the maximum cross section corresponds more closely to this bond energy on a pairwise energy scale, 11.1 eV, Table 1.

Beginning at around 15 eV, a second feature is observed in the CuO^+ cross section. Collection of this product at kinetic energies above 20 eV in the center-of-mass frame varied strongly with experimental conditions (specifically, quadrupole resolution and dc bias) and, hence, is not shown in Fig. 3. Under

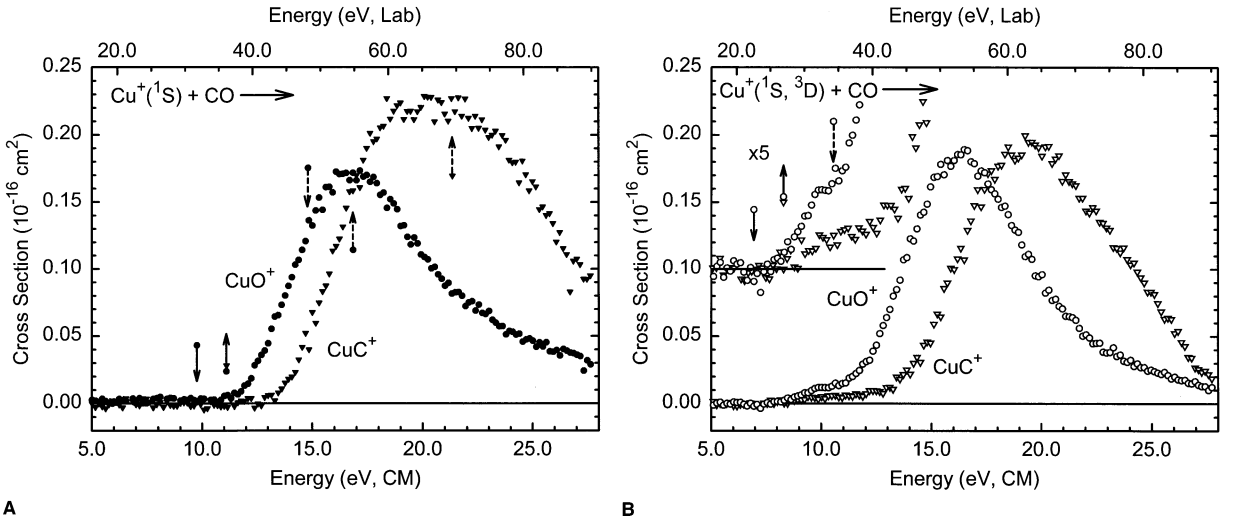

Fig. 2. Variation of the cross sections for reaction of Cu^+ with CO as a function of translational energy in the center-of-mass frame (lower scale) and laboratory frame (upper scale). Data are shown for Cu^+ ions formed by dc discharge with (a) and without (b) the addition of NO to the flow tube. The inset in (b) shows the data on an expanded vertical scale (× 5) and offset from zero. Downward arrows indicate the thermodynamic thresholds for CuO^+ formation from Cu^+ (^1S) and Cu^+ (^3D) at 9.76 (a) and 6.95 (b) eV, respectively. Upward arrows show the thermodynamic thresholds for atomization for reaction with Cu^+ (^1S) and Cu^+ (^3D) at 11.11 (a) and 8.30 (b) eV, respectively. Dashed downward arrows indicate the impulsive thresholds for CuO^+ formation from reaction with Cu^+ (^1S) and Cu^+ (^3D) at 14.8 (a) and 10.6 (b) eV, respectively. Dashed upward arrows in part a show the thresholds for atomization on impulsive energy scales for CuO^+ and CuC^+ at 16.9 and 21.4 eV, respectively. Their counterparts for atomization from Cu^+ (^3D) are shown in (b) at 12.6 and 16.0 eV, respectively.

what we believe to be optimal experimental conditions, we observe that this second feature rises to a maximum of 0.12 ± 0.03 Å^2 at about 33 eV before declining again. This second feature in the CuO^+ cross-section is attributed to reaction (9).

$$Cu^+ + CO_2 \rightarrow CuO^+ + C + O \quad (9)$$

Complete atomization of this system and decomposition of the CuO^+ product formed in reaction (9) can begin at 16.56 eV. However, the peak in the second feature lies well above this energy, but in good agreement with the energy predicted by impulsive behavior, 33.6 eV (Table 1).

Reaction (8) has an apparent threshold of 4–5 eV. The $CuCO^+$ cross section rises to a maximum near 8 eV which must be associated with the dissociation of the $CuCO^+$ ion to $Cu^+ + CO$. This process can begin at D_0(OC–O) but is delayed until about the impulsive value of 7.3 eV, Table 1. As in the CO system, the impulsive model appears to predict the disparate behavior in the peak positions of the two products in this system, neither of which corresponds to D_0(OC–O).

Without NO cooling gas in the flow tube, both the CuO^+ and $CuCO^+$ cross sections are strongly enhanced at low energies (Fig. 3). Note that these excited state cross section features are much larger compared to the ground state cross sections than those in the O_2 and CO systems. The CuO^+ cross section develops a low energy feature having a threshold near 2 eV. The cross section for the $CuCO^+$ channel increases substantially and its threshold also shifts down but not by as much as the CuO^+ channel.

3.4. $Cu^+ + N_2$

The reaction of Cu^+ with N_2 produces only one ionic product, CuN^+, in the endothermic reaction (10).

$$Cu^+ + N_2 \rightarrow CuN^+ + N \quad (10)$$

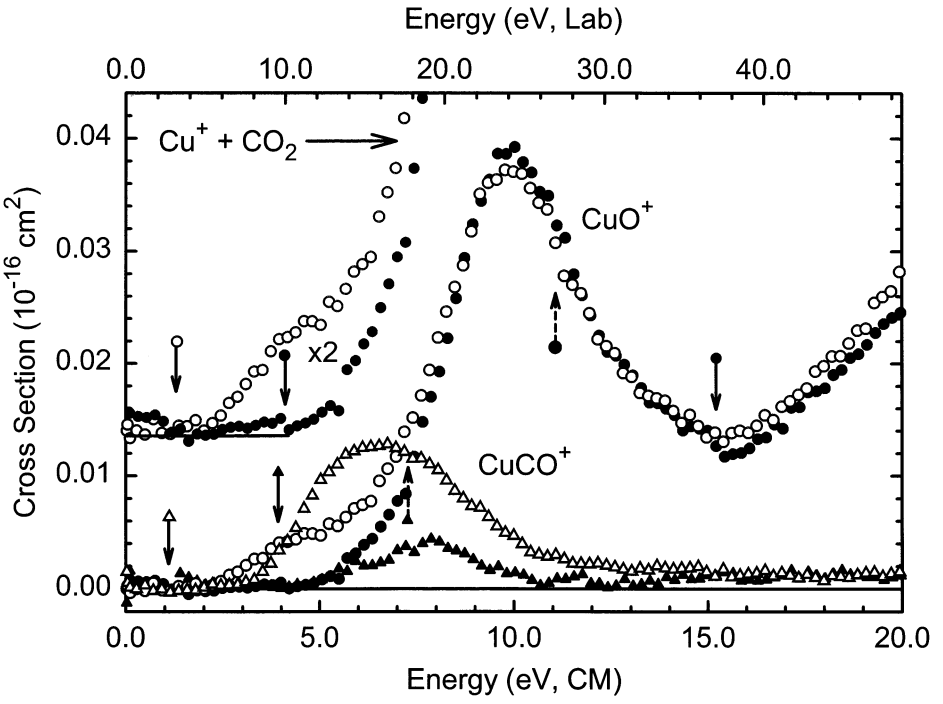

Fig. 3. Variation of the cross sections for reaction of Cu^+ with CO_2 as a function of translational energy in the center-of-mass frame (lower scale) and laboratory frame (upper scale). Data are shown for Cu^+ ions formed by dc discharge with (solid symbols) and without (open symbols) the addition of NO to the flow tube. The inset shows the CuO^+ cross sections on an expanded vertical scale (× 2) and offset from zero. Downward arrows indicate the thermodynamic thresholds for $CuCO^+$ (and CuO^+, inset) formation from Cu^+ (^1S) and Cu^+ (^3D) at 3.91 (4.10) and 1.10 (1.29) eV, respectively. The downward arrow at 15.21 eV indicates the threshold for formation of $CuO^+ + C + O$ from Cu^+ (^1S) reactants. Dashed upward arrows show D_0(OC–O) on impulsive energy scales for $CuCO^+$ and CuO^+ at 7.3 and 11.1 eV, respectively.

The energy dependence of the cross sections for this reaction with Cu^+ produced by dc discharge with and without the addition of NO to the flow tube are shown in Fig. 4. The apparent threshold for reaction of ground state $Cu^+(^1S)$ occurs at ~ 12 eV. The peak of this reaction cross section occurs at ~ 17 eV. The decline in the cross section beyond 17 eV is attributed to reaction (11).

$$Cu^+ + N_2 \rightarrow Cu^+ + N + N \quad (11)$$

As in the CO system, both the threshold and peak energies are well above the bond dissociation energy of the neutral reactant, Table 1. Again, impulsive reactivity appears to quantify this behavior as the onset for reaction (11) in the pairwise energy frame is 16.5 eV, Table 1, in good agreement with the observed peak position (Fig. 3).

Without NO cooling gas added to the flow tube, an appreciable low energy feature in the CuN^+ cross section is observed and can be attributed to the reaction of excited state $Cu^+(^3D)$ with N_2. The apparent threshold for this process occurs at ~ 7 eV.

3.5. $Cu^+ + NO$

The reaction of Cu^+ with NO produces three products formed in reactions (12)–(14).

$$Cu^+ + NO \rightarrow CuO^+ + N \quad (12)$$

$$\rightarrow CuN^+ + O \quad (13)$$

$$\rightarrow NO^+ + Cu \quad (14)$$

Fig. 5(a) shows cross sections determined for these processes for reaction of $Cu^+(^1S)$. Both CuO^+ and

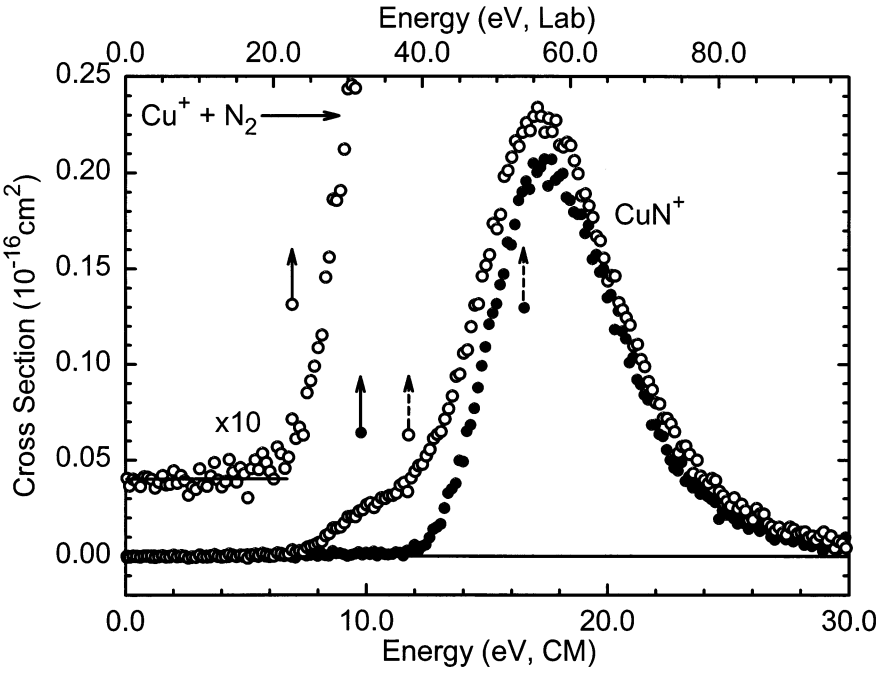

Fig. 4. Variation of the cross sections for reaction of Cu^+ with N_2 as a function of translational energy in the center-of-mass frame (lower scale) and laboratory frame (upper scale). Data are shown for Cu^+ ions formed by dc discharge with (●) and without (○) the addition of NO to the flow tube. The inset shows the data without the addition of NO on an expanded vertical scale (× 10) and offset from zero. Upward arrows show the thermodynamic thresholds for atomization with Cu^+ (^1S) and Cu^+ (^3D) at 9.76 and 6.95 eV, respectively. Dashed upward arrows show the thresholds for $D_0(N_2)$ on an impulsive energy scale for Cu^+ (^1S) and Cu^+ (^3D) at 16.5 and 11.8 eV, respectively.

CuN^+ products have thresholds in excess of the NO bond energy (6.507 eV). The peaks in both cross sections agree very nicely with the pairwise energy predictions of Table 1.

Reaction (14) is simple charge transfer. The ionization energies (IEs) of both Cu and NO are extremely well characterized, 7.726 34 and 9.264 36 eV [48], respectively, such that this process is endothermic by 1.538 eV. The nonzero reactivity observed below this energy is therefore attributed to a trace contaminant in the NO sample, while that above 3 eV corresponds to reaction (14).* Note that the NO^+ cross section reaches a maximum at the onset of reactions (12) and (13). It can be seen that the total reaction cross section rises smoothly from about 4 eV until it reaches a maximum at about 11 eV, the dissociation energy of NO on an impulsive energy scale, Table 1. Thus, the heavy atom transfer processes (12) and (13) compete effectively with the electron transfer process (14). This behavior suggests that the charge transfer process requires an intimate collision between $Cu^+(^1S)$ and NO rather than occurring by a long-range electron jump. This is reasonable considering that the charge transfer is off resonance by 1.5 eV. In this regard, we find it somewhat surprising that the reaction occurs at all and that the observed threshold differs so drastically from the thermodynamic threshold.

When the reactions of $Cu^+(^1S, ^3D)$ are examined, it becomes obvious that the reaction that cools the excited state in the flow tube source is the charge transfer process (Fig. 5(b)). Reaction (14) with $Cu^+(^3D)$ is now exothermic by 1.27 eV and nearly resonant with formation of NO^+ in its fourth vibrational level. Consistent with this, we observe no

* A plausible assignment for this reaction of $Cu^+ + HNO_2 \rightarrow CuOH + NO^+$ was suggested.

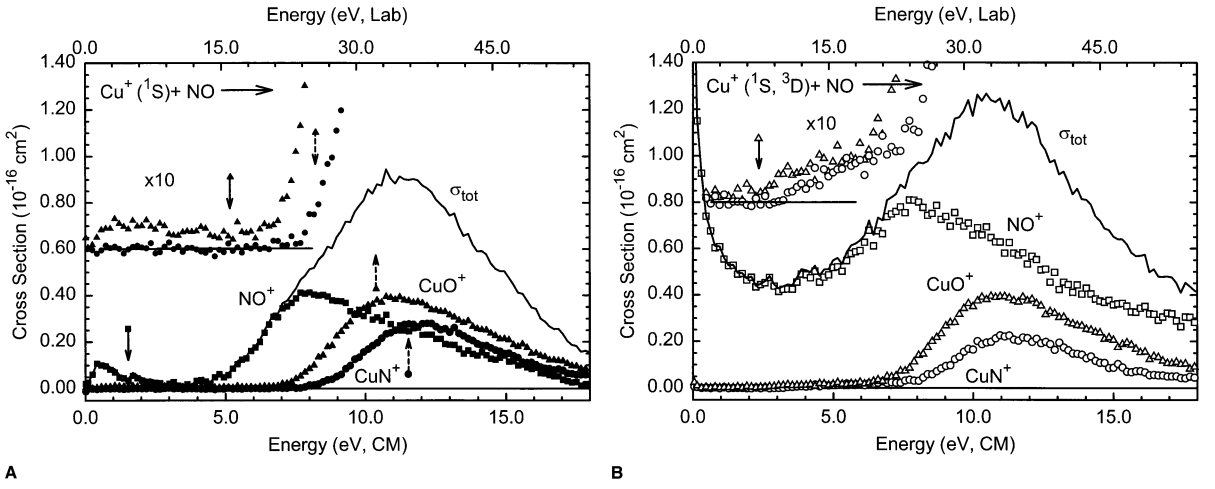

Fig. 5. Variation of the cross sections for reaction of Cu^+ with NO as a function of translational energy in the center-of-mass frame (lower scale) and laboratory frame (upper scale). Data are shown for Cu^+ ions formed by dc discharge with (a) and without (b) the addition of NO to the flow tube. The insets show the data for CuO^+ and CuN^+ on expanded vertical scales (× 10) and offset from zero. Downward arrows indicate the thermodynamic thresholds for CuO^+ formation from Cu^+ (^1S) and Cu^+ (^3D) at 5.16 (a) and 2.35 (b) eV, respectively, NO^+ from Cu^+ (^1S) at 1.54 eV (a). The dashed downward arrow in part a shows the impulsive threshold for CuO^+ formation from Cu^+ (^1S) at 8.2 eV. Dashed upward arrows in (a) show the thresholds for atomization on an impulsive energy scale for CuO^+ and CuN^+ at 10.4 and 11.5 eV, respectively.

energy barrier to this reaction. The energy dependence of this cross section is $E^{-0.35 \pm 0.1}$, declining less rapidly than the Langevin–Gioumousis–Stevenson collision cross section for exothermic ion-molecule reactions, σ_{LGS} [49]. This energy behavior may be an indication that the electron transfer between $Cu^+(^3D)$ and NO does not require an intimate collision of the reactants at higher energies. The magnitude of the exothermic part is approximately $0.023 \pm 0.003\ \sigma_{LGS}$ between 0.05 and 1.0 eV. If the excited state ions present in the reactant ion beam react on every collision, this comparison indicates that the population of $Cu^+(^3D)$ in our beam is about 2%. If the reaction efficiency is less than unity, then the population could be larger, however, the features associated with the ground state reactivity in this and other systems change little in magnitude from those observed with a pure $Cu^+(^1S)$ beam. Thus, the excited state population must be small. Cross sections for the other two products formed in reactions (12) and (13) are nearly identical to those shown in Fig. 5(a), but expansion of these cross sections reveal low energy features, clearly attributable to reaction of $Cu^+(^3D)$.

3.6. $Cu^+ + N_2O$

The reaction of Cu^+ with N_2O yields four products, CuO^+, CuN_2^+, CuN^+, and NO^+ in reactions (15)–(18). Cross sections for these processes from $Cu^+(^1S)$ are shown in Fig. 6.

$$Cu^+ + N_2O \rightarrow CuO^+ + N_2 \quad (15)$$

$$\rightarrow CuN_2^+ + O \quad (16)$$

$$\rightarrow CuN^+ + (N + O) \quad (17)$$

$$\rightarrow NO^+ + CuN \quad (18)$$

The dominant reaction pathways, processes (15) and (16), result from cleavage of the weak N_2–O bond (Table 1) followed by binding one of the fragments to Cu^+. Despite the weakness of this bond, however, reactions of $Cu^+(^1S)$ do not begin until above 1 eV. The energy behavior of the CuO^+ and CuN_2^+ cross sections is complex. Both reactions exhibit two features that can be attributed to reactions (15) and (16), while the CuO^+ cross section has a third feature beginning around 13 eV that is probably associated

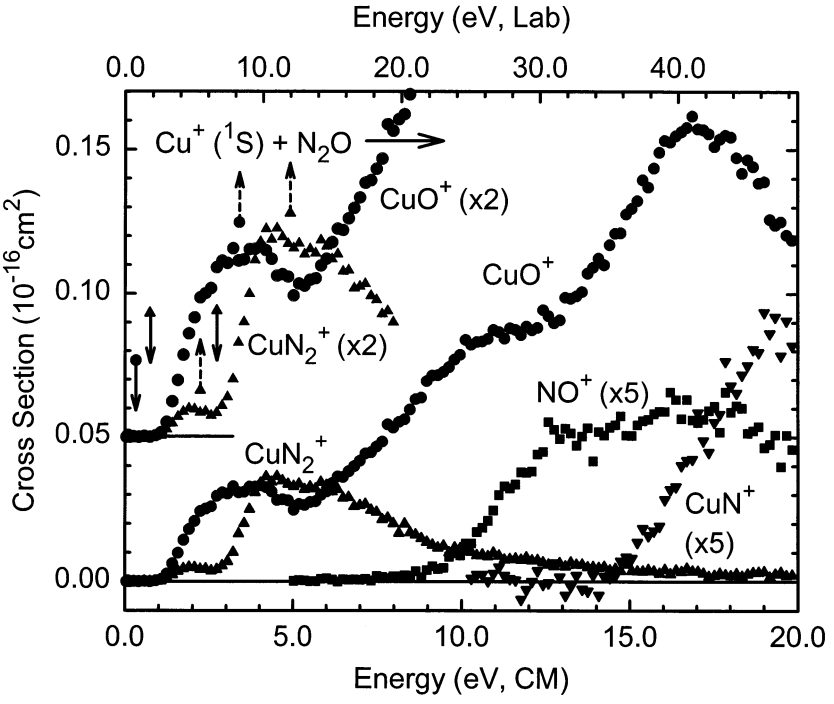

Fig. 6. Variation of the cross sections for reaction of Cu^+ with N_2O as a function of translational energy in the center-of-mass frame (lower scale) and laboratory frame (upper scale). Data are shown for Cu^+ ions formed by dc discharge with the addition of NO to the flow tube. The inset shows the CuO^+ and CuN_2^+ cross sections on an expanded vertical scale (× 2) and offset from zero. The CuN^+ and NO^+ cross sections are expanded by a factor of 5. Downward arrows indicate the thermodynamic thresholds for CuO^+ and CuN_2^+ + O (^3P, ^1D) formation from Cu^+ (^1S) at 0.32, 0.75, and 2.72 eV, respectively. Dashed upward arrows show the thresholds for $D_0[N_2–O\ (^3P)]$ on impulsive energy scales for CuN_2^+ and CuO^+ at 2.2 and 3.4 eV, respectively, and for $D_0[N_2–O\ (^1D)]$ at 4.9 eV.

with formation of CuO^+ + 2N. The lowest energy peaks in both cross sections have maxima that correspond reasonably well with the impulsive predictions for $D_0(N_2–O)$ in Table 1 (Fig. 6). We believe that the second features in these cross sections are associated with dissociation of the N_2–O bond along a singlet surface to form excited state O(^1D). This hypothesis is discussed in detail below.

Two minor products that involve cleavage of the N–N bond of N_2O are also observed at elevated kinetic energies, reactions (17) and (18). The CuN^+ product is not observed until very high energies, above about 14 eV. As formation of Cu^+ + N + NO can occur at 4.92 eV (11.1 eV on an impulsive scale), Table 1, we attribute the observed reactivity to formation of the separated N + O neutral products. Complete atomization of this system can begin at 11.43 eV which suggests that the observed reactivity has a large impulsive component (atomization begins at 25.8 eV on the impulsive scale for CuN^+ formation). Formation of Cu + N + NO^+ is calculated to begin at 6.462 eV (14.6 eV on the impulsive energy scale for CuN = AB). The apparent threshold for this process, ~ 9 eV corresponds with neither of these predictions well, suggesting that the observed process is reaction (18) on an impulsive scale.

When the reactant beam contains excited state $Cu^+(^3D)$ (NO is not used as cooling gas), the CuO^+ and CuN_2^+ cross sections exhibit weak reactivity at thermal energies in addition to the ground state features shown in Fig. 6. The observed behavior indicates that these reactions are now exothermic and have no barriers in excess of the reactant energy, consistent with the low energy thresholds observed for reactions of ground state $Cu^+(^1S)$. Compared to the collision cross section, the magnitudes of these

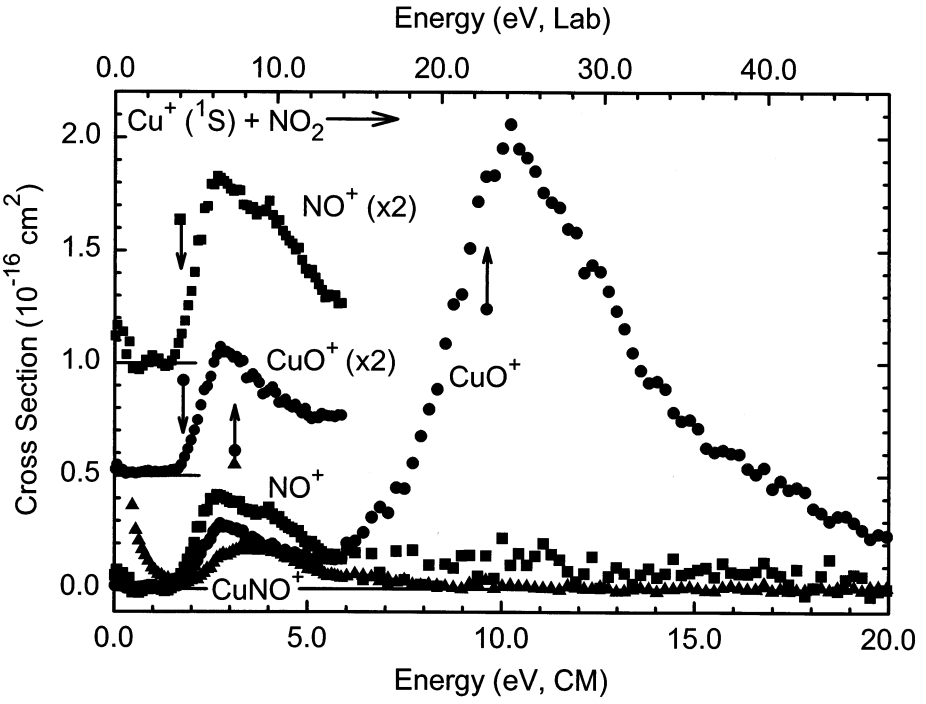

Fig. 7. Variation of the cross sections for reaction of Cu^+ with NO_2 as a function of translational energy in the center-of-mass frame (lower scale) and laboratory frame (upper scale). Data are shown for Cu^+ ions formed by dc discharge with the addition of NO to the flow tube. Insets show the CuO^+ and NO^+ cross sections on expanded vertical scales (× 2) and offset from zero. Downward arrows indicate the thermodynamic thresholds for NO^+ and CuO^+ formation from Cu^+ (^1S) at 1.72 and 1.77 eV, respectively. Upward arrows show the thermodynamic thresholds for D_0(ON–O) at 3.116 eV and for atomization at 9.623 eV.

cross sections are 0.011 ± 0.002 σ_{LGS} and 0.004 ± 0.001 σ_{LGS}, respectively, below 0.1 eV. If $Cu^+(^3D)$ reacts with unit efficiency, this indicates that there is approximately 1.5% of this excited state present in this beam, comparable to the 2% figure noted above. We also observe formation of an CuN_2O^+ adduct at thermal energies. The cross section for this process depends linearly on the N_2O pressure, indicating that this adduct is formed by collisional stabilization in sequential bimolecular reactions. Both the CuN^+ and NO^+ cross sections exhibit low energy, endothermic features when the Cu^+ excited state is present. The apparent thresholds for both of these features are much lower than those for ground state Cu^+ (by about 10 and 7 eV, respectively), clearly indicating that the ground state thresholds do not have a thermodynamic meaning.

3.7. $Cu^+ + NO_2$

The reaction of Cu^+ with NO_2 yields three products formed in reactions (19)–(21).

$$Cu^+ + NO_2 \rightarrow CuO^+ + NO \quad (19)$$

$$\rightarrow CuNO^+ + O \quad (20)$$

$$\rightarrow NO^+ + CuO \quad (21)$$

Cross sections for these processes from $Cu^+(^1S)$ are shown in Fig. 7. In contrast to all other systems in this study, the cross sections observed in this system behave as expected based on known thermochemistry. For example, both the CuO^+ and $CuNO^+$ products can dissociate to form Cu^+ beginning at the ON–O bond energy of 3.116 eV (Table 1). The cross sections for both of these products are observed to reach

maxima near this energy. Further, atomization of this system to form $Cu^+ + N + 2O$ can begin at 9.623 eV (Table 1), consistent with the higher energy peak in the CuO^+ cross section. Thus, the second feature in the CuO^+ cross section can be attributed to formation of $CuO^+ + N + O$. Based on thermochemistry compiled by Lias et al. [48], the ionization energy of CuO is 9.23 ± 0.55 eV, very similar to IE(NO) = 9.264 36 eV, which means that reactions (19) and (21) are nearly isoenergetic. This is consistent with the observed behavior in the cross sections for NO^+ and the low energy feature for CuO^+. Some reactivity is observed below about 1.5 eV in the $CuNO^+$ and NO^+ channels (the latter has been modeled and removed from Fig. 7), but this is attributable to contaminants in the NO_2 sample, as the magnitudes of these cross sections increased during the course of the experiments.

When the Cu^+ beam contains excited states, we observe that both the CuO^+ and NO^+ cross sections develop tails at thermal energies indicative of exothermic reactivity. At higher energies (above 1.5 eV), these cross sections remain the same as shown in Fig. 7. In contrast, the $CuNO^+$ reaction cross section does not change over the entire energy range examined. Unfortunately, contamination of the NO_2 (which affects primarily the NO^+ and $CuNO^+$ channels) precludes a meaningful analysis of the magnitudes of the observed exothermic reactivity.

4. Discussion

4.1. Electronic states of the products

One consideration in understanding the results of the present study is the electronic states of the copper containing products. These include the diatomics, CuC^+, CuN^+, CuN, CuO^+, and CuO, and the triatomics, $CuCO^+$, CuN_2^+, and $CuNO^+$. Unfortunately, except for CuO, no experimental characterization of the electronic states of these species is available to our knowledge. The first two triatomics almost certainly have $^1\Sigma^+$ ground states formed by adding the $^1\Sigma^+$ ground state of CO or N_2 molecules to the $Cu^+(^1S)$ ground state in an end-on geometry. This has been confirmed by ab initio calculations in the case of $CuCO^+$ [50]. It is not clear whether the geometry of $CuNO^+$ will be linear or bent, especially as no covalent bond formation is expected. However, it is equally clear that $CuNO^+$ should have a doublet ground state corresponding to association of $Cu^+(^1S)$ and $NO(^2\Pi)$. For the diatomics, we rely on extrapolating information from the known spectroscopy of CuO [51]. CuO has a $^2\Pi$ ground state with a $(1\delta^4)(3\pi^4)(8\sigma^2)(9\sigma^2)(4\pi^3)$ electron configuration. For this late first row metal, the 1δ, 3π, and 8σ orbitals are largely $3d$-like metal orbitals (nearly core orbitals), the 9σ is a bonding orbital between the $4s$ orbital on Cu and the $2p\sigma$ orbital on O, and the 4π is largely O $2p\pi$ although there is some antibonding character. Ionization of this species should give a $^3\Sigma^-$ ground state having a $(1\delta^4)(3\pi^4)(8\sigma^2)(9\sigma^2)(4\pi^2)$ configuration. Indeed, ionization should contract the $3d$ orbitals, further isolating them from the O-based orbitals. Note that this configuration can be viewed as simple association of $Cu^+(^1S, 3d^{10})$ with $O(^3P, 2p^4)$ such that the lone pair of electrons on O is pointed at the Cu^+ ion. This ground state configuration has been verified by ab initio calculations which also identify a $^3\Pi[(1\delta^4)(3\pi^4)(8\sigma^2)(9\sigma^1)(4\pi^3)]$ state as the first excited state, lying 0.8 [52] and 1.03 eV [53] higher in energy.

As CuN and CuO^+ are isoelectronic, it seems relatively certain that CuN also has a $^3\Sigma^-$ ground state. Ionization of CuN could form CuN^+ in a $^2\Pi[(1\delta^4)(3\pi^4)(8\sigma^2)(9\sigma^2)(4\pi^1)]$ or $^4\Sigma^-[(1\delta^4)(3\pi^4)(8\sigma^2)(9\sigma^1)(4\pi^2)]$ state. The latter is probably the ground state as it correlates to separated $Cu^+(^1S, 3d^{10})$ + $N(^4S, 2p^3)$ ground state atoms, while the $^2\Pi$ state correlates to the excited $N(^2P, 2p^3)$ state, which lies 2.38 eV higher in energy [38]. Removing another electron from this orbital scheme to generate CuC^+ suggests possible states of $^1\Sigma^+$ $[(1\delta^4)(3\pi^4)(8\sigma^2)(9\sigma^2)(4\pi^0)]$, $^3\Pi$ $[(1\delta^4)(3\pi^4)(8\sigma^2)(9\sigma^1)(4\pi^1)]$, or $^3\Sigma^-$ $[(1\delta^4)(3\pi^4)(8\sigma^2)(9\sigma^0)(4\pi^2)]$. Only the latter two states correlate with ground state separated atoms, $Cu^+(^1S)$ + $C(^3P, 2p^2)$. It seems likely that one of the $C(2p)$ electrons would point towards the Cu^+, such that the $^3\Pi$ state is the probable ground state.

Table 2
Spin conservation in reactions of $Cu^+(^1S)$

Reactant	Ionic product	Neutral product	Spin-allowed[a]
O_2 ($^3\Sigma_g^-$)	CuO^+ ($^3\Sigma^-$)	O (^3P)	yes
CO ($^1\Sigma^+$)	CuO^+ ($^3\Sigma^-$)	C (^3P)	yes
	CuC^+ ($^3\Pi$)	O (^3P)	yes
CO_2 ($^1\Sigma_g^+$)	CuO^+ ($^3\Sigma^-$)	CO ($^1\Sigma^+$)	CuO^+ ($^1\Delta$)
	$CuCO^+$ ($^1\Sigma^+$)	O (^3P)	O (^1D)
N_2 ($^1\Sigma_g^+$)	CuN^+ ($^4\Sigma^-$)	N (^4S)	Yes
NO ($^2\Pi$)	CuO^+ ($^3\Sigma^-$)	N (^4S)	Yes
	CuN^+ ($^4\Sigma^-$)	O (^3P)	Yes
N_2O ($^1\Sigma^+$)	CuO^+ ($^3\Sigma^-$)	N_2 ($^1\Sigma_g^+$)	CuO^+ ($^1\Delta$)
	CuN_2^+ ($^1\Sigma^+$)	O (^3P)	O (^1D)
	CuN^+ ($^4\Sigma^-$)	NO ($^2\Pi$)	CuN^+ ($^2\Pi$)
	NO^+ ($^1\Sigma^+$)	CuN ($^3\Sigma^-$)	CuN ($^1\Delta$)
NO_2 ($^2A_1$)	CuO^+ ($^3\Sigma^-$)	NO ($^2\Pi$)	yes
	$CuNO^+$ (^2A)	O (^3P)	yes
	NO^+ ($^1\Sigma^+$)	CuO ($^2\Pi$)	yes

[a] When the reaction is spin forbidden to form ground state products, an excited state of the products that makes the reaction spin allowed is provided.

On the basis of these considerations, we assume in the following discussion that the ground states of CuO^+ and CuN are $^3\Sigma^-$; that of CuN^+ is $^4\Sigma^-$; CuC^+, $^3\Pi$; $CuCO^+$ and CuN_2^+, $^1\Sigma^+$; and $CuNO^+$, ^2A. Table 2 summarizes the electronic states for the reactions of $Cu^+(^1S)$ with the molecules considered here and the ground state products. We find that spin can be conserved in all reactions of $Cu^+(^1S)$ studied here except those for CO_2 and N_2O. In contrast, reactions of $Cu^+(^3D)$ are spin allowed for all reactions including those with CO_2 and N_2O. We believe that the inability to conserve spin in the cases of the $Cu^+(^1S)$ + CO_2 and N_2O reactions is probably the key reason that the magnitude of the CuO^+ cross sections are so much smaller than in the other systems. For instance, in the CO_2 system, the CuO^+ cross section is 50 times smaller than in the O_2 system (even though the neutral reactant bond energies are similar, Table 1) and 10 times smaller than the CO and NO systems, where the bonds being broken are stronger. Further, the small magnitudes of the $CuCO^+$ and CuN_2^+ cross sections from $Cu^+(^1S)$ are consistent with the spin-forbidden character of this reaction. In addition, these reactions are spin allowed with $Cu^+(^3D)$, accounting for the much larger relative magnitudes of the excited state cross section features compared to the other systems.

Spin conservation also provides a ready explanation for the two features observed in the CuN_2^+ product formed in the N_2O system (Fig. 6(a)). As noted in Table 2, this reaction can become spin-allowed for the $Cu^+(^1S)$ reactant if the neutral oxygen atom product is formed in its first excited ^1D state, lying 1.97 eV above the ^3P ground state [38]. Thus, we attribute the small low energy feature to the spin-forbidden formation of CuN_2^+ ($^1\Sigma^+$) + O (^3P) and the higher energy feature beginning about 3 eV to the spin-allowed formation of CuN_2^+ ($^1\Sigma^+$) + O (^1D). Additional evidence for this assignment comes from analysis of the dissociation energies to form Cu^+ + N_2 calculated on a pairwise energy scale, 2.2 and 4.9 eV (Table 1), respectively. These energies correspond nicely with the peaks observed for the two features in the CuN_2^+ cross section (Fig. 6(a)). It seems probable that the first and second features in the CuO^+ cross section, where the second feature is also much larger than the lower energy feature, can also be attributed to spin-forbidden and spin-allowed reactions, respectively. Indeed, the first feature in the CuO^+ cross section occurs close to the pairwise dissociation threshold of 3.4 eV (Table 1) expected for $Cu^+(^1S)$ + $O(^3P)$ + $N_2(^1\Sigma_g^+)$, a spin-forbidden reaction. The higher energy feature beginning around 5 eV would involve spin-allowed formation of an excited singlet state of CuO^+ (Table 2) as excited triplet states of N_2 are too high in energy. This is discussed further below.

4.2. CuO^+ and CuO thermochemistry

Of all the reactions of $Cu^+(^1S)$ examined in this study, the NO_2 system is the only one where impulsive reactivity is not present. Thus, this system offers the best opportunity to obtain good thermodynamic information. The cross sections for reactions (19) and (21) were analyzed using Eq. (2). When n is allowed to vary freely, we find an optimum value of about 0.9, therefore, we also analyzed the data using the line-of-centers cross section, $n = 1$. The optimized parameters given in Table 3 are the average of these two

Table 3
Optimized parameters of Eq. (2)

Reactants	Ionic product	σ_0	n	E_0, eV	p	E_D, eV
$Cu^+(^1S) + O_2$	CuO^+	0.11 (0.01)	3.4 (0.1)	3.50 (0.06)	3	7.4
$Cu^+(^3D) + O_2$	CuO^+	0.035 (0.007)	2.2 (0.1)	0.79 (0.07)	2	2.3
$Cu^+(^1S) + CO$	CuO^+	1.00 (0.57)	1.0 (0.1)	12.06 (0.20)	2	17.0 (0.6)
	CuC^+	0.88 (0.25)	1.0 (0.2)	13.84 (0.40)	2	20.5 (1.2)
$Cu^+(^1S) + CO_2$	CuO^+	0.038 (0.057)	3.1 (0.7)	3.84 (1.02)		
	$CuCO^+$	0.008 (0.003)	1.1 (0.2)	4.63 (0.63)	2	7.9 (0.1)
$Cu^+(^3D) + CO_2$	CuO^+	0.012 (0.010)	1.5 (0.4)	1.91 (0.55)		
	$CuCO^+$	0.030 (0.014)	1.1 (0.4)	3.4 (0.4)	2	6.9 (0.2)
$Cu^+(^1S) + N_2$	CuN^+	0.40 (0.08)	1.5 (0.1)	12.57 (0.13)	2	16.8 (0.2)
$Cu^+(^3D) + N_2$	CuN^+	0.06 (0.04)	1.3 (0.4)	7.02 (0.46)	1	13.7
$Cu^+(^1S) + NO$	CuO^+	1.39 (0.28)	1.0 (0.2)	7.52 (0.16)	1	10.8 (0.3)
	CuN^+	0.93 (0.28)	1.0 (0.2)	8.43 (0.24)	1, 2	11.7 (0.4)
	NO^+	0.51 (0.37)	1.6 (0.6)	4.14 (0.61)		7.7 (0.3)
$Cu^+(^3D) + NO$	CuO^+	0.030 (0.006)	1.0 (0.1)	2.26 (0.19)		
	CuN^+	0.032 (0.004)	1.0	2.17 (0.11)		
$Cu^+(^1S) + N_2O$	CuO^+	0.060 (0.003)	0.8 (0.1)	1.33 (0.05)	1, 2	4.5 (0.3)
	CuN_2^+	0.014 (0.001)	0.4 (0.1)	1.29 (0.08)	1, 2	2.4 (0.2)
	CuN_2^+	0.09 (0.03)	1.2 (0.7)	2.72 (0.31)	1, 2	5.4 (0.3)
	CuN^+	0.145 (0.097)	0.7 (0.4)	15.67 (1.22)		
	NO^+	0.058 (0.019)	0.7 (0.2)	9.84 (0.37)	1, 2	18.2 (1.1)
$Cu^+(^3D) + N_2O$	CuN^+	0.18 (0.07)	1.3 (0.4)	5.36 (0.29)	1, 2	9.5 (0.7)
	NO^+	0.002 (0.001)	2.0 (0.1)	3.15 (0.29)		
$Cu^+(^1S) + NO_2$	CuO^+	0.87 (0.52)	1.2 (0.4)	1.77 (0.12)	1, 2	3.1 (0.6)
	NO^+	1.17 (0.48)	0.9 (0.3)	1.72 (0.12)	1, 2	3.1 (0.4)

approaches. We find that both reactions have the same threshold within experimental error. This is consistent with the observed behavior as the two cross sections mimic one another closely in the threshold region. The NO^+ cross section is slightly bigger, consistent with a slightly lower threshold. Given $D_0(ON–O) = 3.116 \pm 0.008$ eV (Table 1), the threshold for reaction (19) can be converted using the formula, $D_0(Cu^+–B) = D_0(BC) - E_0(CuB^+)$ where $B = O$ and $C = NO$ in this system, to $D_0(Cu^+–O) = 1.35 \pm 0.12$ eV. Given the IEs of NO and Cu provided above, the threshold for reaction (21) yields $D_0(Cu–O) = 2.94 \pm 0.12$ eV. (This latter value agrees with a preliminary report for this bond energy obtained from analysis of this same reaction seven years ago in our laboratory, 2.85 ± 0.15 eV [54]. This earlier work was conducted with a Cu^+ beam that contained excited states and, hence, this threshold determination is not as reliable as the present value.) When this new value is combined with our value for $D_0(Cu^+–O)$, we obtain $IE(CuO) = 9.32 \pm 0.17$ eV. We can also independently determine the average of the difference in the thresholds for the two channels, which is more precise than the difference in the absolute threshold determinations. When n is held to unity, we find that the NO^+ threshold lies 0.08 ± 0.06 eV lower than the CuO^+ threshold, consistent with the absolute thresholds given in Table 3. This value defines the difference in IEs of NO and CuO, which gives $IE(CuO) = 9.34 \pm 0.06$ eV.

The value reported here for $D_0(CuO)$ compares well with literature information, although this is sparse. In the critical review of Pedley and Marshall [55], they cite 2.76 ± 0.22 eV, a value taken exclusively from the work of Smoes et al. [56]. Recently, Watson et al. [57] restudied the equilibrium used by Smoes et al. to measure $D(CuO)$. They found that second and third law values for the heat of formation of CuO at 298 K varied widely, 329 ± 5 and 433 ± 33 kJ/mol (corresponding to 0 K bond energies of

Table 4
Thermodynamic and pairwise threshold energies for reaction of $Cu^+(^1S, ^3D^*)$

Reactant (BC)	Products (AB + C)	Mass factor[a]	E_0(AB) eV[b]	E_0^*(AB) eV[c]	E_{0P}(AB) eV[d]	E_{0P}^*(AB) eV[e]
O_2	$CuO^+ + O$	1.663	3.77	0.96	6.3	1.6
CO	$CuO^+ + C$	1.519	9.76	6.95	14.8	10.6
CO_2	$CuO^+ + CO$	2.030	4.10	1.29	8.3	2.6
	$CuO^+ + C + O$	2.030	15.21	12.40	30.9	25.2
	$CuCO^+ + O$	1.336	3.91	1.10	5.2	1.5
	$CuCO^+ + O(^1D)$	1.336	5.88	3.07	7.9	4.1
NO	$CuO^+ + N$	1.593	5.16	2.35	8.2	3.7
	$NO^+ + Cu$		1.538	< 0		
N_2O	$CuO^+ + N_2$	2.030	0.32	< 0	0.6	< 0
	$CuN_2^+ + O(^3P)$	1.336	0.75	< 0	1.0	< 0
	$CuN_2^+ + O(^1D)$	1.336	2.72	< 0	3.6	< 0
NO_2	$CuO^+ + NO$	2.083	1.77	< 0	3.7	< 0
	$CuO^+ + N + O$	2.083	8.27	5.46	17.2	11.4
	$NO^+ + CuO$	2.083	1.72	< 0	3.6	< 0

[a] The mass factor in Eq. (1): $(A + B)(B + C)/B(A + B + C)$.
[b] $E_0(AB) = D_0(BC) - D_0(AB)$.
[c] $E_0^*(AB) = D_0(BC) - D_0(AB) - E^*(^3D)$.
[d] $E_{0P}(AB) = E_0(AB) \times (A + B)(B + C)/B(A + B + C)$.
[e] $E_{0P}^*(AB) = E_0^*(AB) \times (A + B)(B + C)/B(A + B + C)$.

2.64 and 1.56 eV, respectively), indicating that equilibrium was probably established only over a very narrow range of temperatures. Because of these difficulties, Watson et al. recommended the preliminary value of Clemmer et al. [54] as the best experimental value available. Additional evidence that the bond energy from Smoes et al. is probably low comes from Vinckler et al. [58] who found that the reaction of Cu with NO_2 is near thermoneutral from 303 to 762 K, indicating that $D(CuO) \approx D_0(ON–O) = 3.116 \pm 0.008$ eV. We note that our value is in reasonable agreement with this observation and a theoretical value of 2.79 eV [59] and that our ionization energy for CuO agrees with the direct determination of Watson et al., 9.1 ± 0.5 eV, and a calculated value of 9.15 eV [53].

Even less thermodynamic information concerning CuO^+ is available in the literature. The compilation of Lias et al. [48] cites limits determined by Kappes and Staley [34]. They found that Cu^+ reacted at thermal energies with O_3 to form CuO^+ but not with N_2O or O_2, consistent with the observations of this study. They concluded that $D(O_2–O) < D(Cu^+–O) < D(N_2–O)$ placing the copper oxide cation bond energy between 1.1 and 1.7 eV, consistent with the 1.35 ± 0.12 eV value determined here. The only other value in the literature comes from our previous work on the reaction of Cu^+ with O_2 [5], where we determined $D_0(Cu^+–O) = 1.62 \pm 0.15$ eV. We now believe that this value is flawed because of the influence of the impulsive reactivity on the shape of the reaction cross section for process (3). This hypothesis is explored further in the next section.

4.3. Analysis of reactions with O_2, CO, NO, and N_2

Copper monoxide cations are formed in most of the systems studied here. As noted in the Results section, the cross sections for formation of CuO^+ exhibit signs of impulsive reactivity in all but the NO_2 system, analyzed in detail in the previous section. Because of this, it is unlikely that analysis of the kinetic energy dependence of these cross sections will provide useful thermodynamic information. However, it is still of interest to examine how the thresholds obtained agree with thermodynamic and impulsive predictions. On the basis of $D_0(Cu^+–O) = 1.35 \pm 0.12$ eV, these predictions are summarized in Table 4.

In the O_2 system, analysis of the CuO^+ cross section with Eq. (2) over the kinetic energy range from threshold to the maximum yields the optimum parameters listed in Table 3. These agree very well with values published previously for the reaction of O_2 with $Cu^+(^1S)$ formed by surface ionization [5]. As in that work, this threshold corresponds to $D_0(Cu^+–O) = 1.62 \pm 0.06$ eV, which we now believe is too high, i.e. the threshold is too low. We believe that this analysis is flawed because there is both a thermodynamic and an impulsive reaction component to the cross section for CuO^+ formation. This is obvious from the good agreement between the energy of the peak in the cross section and the impulsive prediction for the onset of reaction (4) (Fig. 1). When Eq. (2) is used to model the sum of the thermodynamic and impulsive processes, a large value for the parameter n (Table 3) is needed to reproduce the cross section up to its maximum. This large value of n is accompanied by a low E_0 value, i.e. one below the value based on a bond energy of 1.35 ± 0.12 eV, $E_0 = 3.77 \pm 0.12$ eV (Table 4). This high value of n contrasts with values near 2 that were needed to reproduce the cross sections for most other first row transition metal cations reacting with O_2, which exhibit no signs of impulsive reactivity [5]. Indeed, we find that the CuO^+ cross section can be modeled very well at energies below $D_0(O_2)$ using Eq. (2) with n held to 2 and E_0 held to 3.77 eV. In other words, in the region attributable to thermodynamic reactivity (below 5 eV), the behavior of the cross section is comparable to those for other transition metal cations. At higher energies, a second model representing the impulsive reactivity must then be used to reproduce the CuO^+ cross section to its maximum and beyond. It seems clear that although the $Cu^+(^1S) + O_2$ reaction can proceed at its thermodynamic limit, there is substantial impulsive character to this reaction (perhaps increasing with increasing kinetic energy). In the end, we conclude that the impulsive reactivity precludes obtaining accurate thermodynamic information from the $Cu^+(^1S) + O_2$ system.

When excited states are present in the Cu^+ beam, reaction with O_2 yields a distinct feature at low energies that peaks at the thermodynamic (*not* impulsive) threshold for reaction (4) (Fig. 1). Analysis of the low energy feature in the CuO^+ cross section using Eq. (2) yields the optimum parameters in Table 3. The threshold obtained lies 2.98 ± 0.17 eV below the thermodynamic threshold for reaction of $Cu^+(^1S)$, confirming that this feature is primarily because of the reaction of $Cu^+(^3D)$, $E^* = 2.81$ eV. Also, the value of n lies close to 2, consistent with the expected behavior for $M^+ + O_2$ reactions [5]. Conversely, one can use this threshold to derive $D_0(Cu^+–O) = 1.52 \pm 0.07$ eV, in reasonable agreement with the value of 1.35 ± 0.12 eV derived from the NO_2 system. Because higher lying states of Cu^+ may be present in the reactant beam, the 1.52 eV bond energy is best viewed as an upper limit.

In the CO system, the thermodynamic threshold for reaction (5) is 9.76 ± 0.12 eV (14.8 ± 0.2 eV in the impulsive limit) (Table 4). Analysis of this cross section with Eq. (2) yields a threshold of 12.1 ± 0.2 eV (Table 3). This intermediate value indicates that the observed reactivity is neither completely thermodynamic nor impulsive (as in the O_2 system). This means that acquiring precise thermodynamic information from thresholds exhibiting such dynamic behavior is not possible. We also note that the optimum value of n (Table 3) is very close to unity, i.e. the line-of-centers cross section. This is reasonable as impulsive collisions of hard spheres are accurately described by the line-of-centers cross section function. For the CuC^+ channel, we measure a threshold that lies a factor of 1.15 higher than that for CuO^+ (Table 3), but when converted to E(pair) values using Eq. (1), the threshold for CuC^+ (7.2 ± 0.2 eV) lies below that for CuO^+ (7.9 ± 0.1 eV). Hence, the reaction of $Cu^+(^1S)$ + CO does not let us reliably determine whether $D(CuC^+)$ is greater or less than $D(CuO^+)$.

When $Cu^+(^3D)$ is present in the reactant ion beam, small low energy features appear in the CuO^+ and CuC^+ cross sections. These are sufficiently small that we restrict analysis of these features with Eq. (2) by holding $n = 1$. These analyses yield approximate thresholds of 8.5 ± 0.2 and 8.3 ± 0.2 eV for the two products, respectively. Again these thresholds cannot be converted to reliable thermodynamic information

as they lie above $D_0(CO) - E^*(^3D) = 8.3$ eV. However, these results do suggest that the copper oxide and copper carbide cation bond energies are probably similar.

In the NO system, the thermodynamic threshold for CuO^+ formation is 5.16 ± 0.12 eV, while on the pairwise energy scale it is predicted to be 8.2 ± 0.2 eV (Table 4). Again the measured threshold of 7.52 ± 0.16 eV (Table 3) for reaction of $Cu^+(^1S)$ lies between these limiting values. We also measure that the threshold for CuN^+ formation lies at 8.43 ± 0.24 eV. If we convert these measured thresholds from E_0(CM) values to E_0(pair) using Eq. (1), we obtain 4.72 ± 0.10 and 4.75 ± 0.14 eV, respectively, i.e. nearly identical values. Although such an interpretation is highly speculative, this result suggests that the Cu^+–N and Cu^+–O bond energies are comparable.

For reaction with NO, the thermodynamic threshold for CuO^+ production from $Cu^+(^3D)$ [$E^* = 2.81$ eV] is 2.35 ± 0.12 eV, close to the apparent threshold in this cross section (Fig. 5(b)). Indeed, analysis provides a threshold of 2.26 ± 0.19 eV (Table 3), which corresponds to a Cu^+–O bond energy of 1.44 ± 0.19 eV, in good agreement with the 1.35 ± 0.12 eV value measured in the NO_2 system. Likewise, the threshold measured for formation of CuN^+ is 2.17 ± 0.11 eV, such that $D_0(Cu^+–N) = 1.53 ± 0.11$ eV. Although such a result is not considered definitive because of the uncertainty in the Cu^+ electronic state distribution, we again find that the CuN^+ and CuO^+ bond energies are similar, helping to substantiate the analysis of the impulsive behavior for reaction of $Cu^+(^1S)$ discussed previously.

In the N_2 system, analysis of the CuN^+ cross section with Eq. (2) yields the optimum parameters given in Table 3, including a threshold that lies above $D_0(N_2)$. If we speculatively convert the measured threshold using Eq. (1) to E_0(pair), we obtain 7.43 ± 0.08 eV, which corresponds to $D_0(Cu^+–N) = 2.3 ± 0.1$ eV. This value is higher than that obtained from reaction of NO with $Cu^+(^3D)$ and seems much too high compared with $D_0(Cu^+–O) = 1.35$ eV. Therefore, as in the CO and NO reaction systems, the threshold for formation of CuN^+ falls in between the thermodynamic and purely impulsive values such that no useful thermochemistry can be acquired at this time.

Reaction of $Cu^+(^3D)$ with N_2 yields a distinct low energy feature that can be analyzed as shown in Table 3. However, this threshold again lies below the onset for dissociation of the CuN^+ product, $D_0^*(N_2) = 6.95$ eV, indicating that no useful thermodynamic information can be obtained.

4.5. Analysis of reactions with N_2O

Although N_2O has the weakest oxide bond energy of the systems examined here (Table 1), previous studies have demonstrated that there can be a bottleneck in the abstraction of an oxygen atom from N_2O reactions by transition metal cations [60]. This bottleneck is attributed to the fact that $N_2O(^1\Sigma^+)$ cannot dissociate to the ground state species, $N_2(^1\Sigma_g^+)$ + $O(^3P)$, along a spin-allowed pathway, but rather to $N_2(^1\Sigma_g^+)$ + $O(^1D)$, 1.97 eV higher in energy [38]. Evidence for this bottleneck in the present work comes from analysis of the CuO^+ cross section (Table 3). The observed threshold of 1.33 ± 0.05 eV is well above the thermodynamic threshold for CuO^+ production in reaction (15), 0.32 ± 0.12 eV (Table 4), and well above the predicted threshold on an impulsive scale, 0.65 ± 0.24 eV (Table 4). However, if we use the diabatic, spin-allowed bond energy for N_2O, 1.672 + 1.97 = 3.64 eV, then the predicted thresholds for CuO^+ are 2.29 ± 0.12 and 4.65 ± 0.24 eV, which are much higher than the measured value. While this could again be a consequence of mixed thermodynamic and impulsive behavior, we believe that the measured threshold for this reaction reflects a barrier along the potential energy surface that represents the crossing between the singlet and triplet surfaces for N_2–O dissociation as perturbed by the presence of Cu^+.

Additional evidence for the presence of such a barrier is the observation that the thresholds for reactions (15) and (16) are essentially identical (Table 3). If this result had thermodynamic meaning, then this would indicate that the dative Cu^+–N_2 bond energy is the same as the covalent Cu^+–O bond energy (1.35 ± 0.12 eV). However, it seems unlikely

that $D_0(Cu^+–N_2)$ should nearly equal $D_0(Cu^+–CO) = 1.54 \pm 0.07$ eV [37]. Indeed, previous measurements of $M^+–N_2$ and $M^+–CO$ bond energies for M = Fe and Ni find the former are about 60% of the latter [61,62]. In addition, the measured threshold of 1.29 ± 0.08 eV (Table 3) would correspond to $D_0(Cu^+–N_2) = 0.38 \pm 0.08$ eV, which is much too low, also consistent with the presence of a barrier. Additional confirmation of this hypothesis comes from an understanding of the second feature in the CuN_2^+ cross section. As discussed earlier, this can be attributed to reaction along the singlet surface of the N_2O dissociation such that the product in reaction (16) is $O(^1D)$, making the reaction spin-allowed (Table 2). Support for this assignment comes from the correspondence of the peaks in the two features of the CuN_2^+ cross section with the impulsive dissociation energies for $O(^3P)$ and $O(^1D)$ formation (Table 1, see discussion above). The threshold measured for the second cross section feature (using Eq. (2) with n allowed to vary and held to unity) is 2.72 ± 0.31 eV (Table 3). This corresponds to $D_0(Cu^+–N_2) = D_0(N_2–O) + E^*[O(^1D)] - E_0(15) = 0.92 \pm 0.31$ eV, about 60% of $D_0(Cu^+–CO)$, which seems reasonable although this assignment is somewhat speculative.

The second feature observed in the CuO^+ cross section starting near 5 eV (Fig. 6(a)) probably corresponds to formation of $CuO^+ + N_2$ and seems likely to be associated with a spin-allowed pathway for formation of these final products. This must mean that a singlet state of CuO^+ is formed and that the reaction couples with the singlet surface for N_2–O dissociation. Calculations find that the lowest singlet state of CuO^+ is the $^1\Delta$, lying 1.4 [52] or 1.08 [53] eV above the $^3\Sigma^-$ ground state. Thus, the thermodynamic threshold for formation of $CuO^+(^1\Delta) + N_2\ (^1\Sigma_g^+)$ relative to the N_2–$O(^1D)$ dissociation energy of 3.64 eV is 3.7 or 3.37 ± 0.12 eV (7.5 or 6.8 ± 0.2 eV on an impulsive energy scale). If orbital and spin angular momentum are conserved, then reaction of $Cu^+(^1S) + N_2O(^1\Sigma^+)$ will form $CuO^+(^1\Sigma^+) + N_2(^1\Sigma_g^+)$. Calculations indicate that the $CuO^+(^1\Sigma^+)$ state lies 2.9 [52] or 1.64 [53] eV above the $^3\Sigma^-$ ground state such that this threshold lies at 5.2 or 3.9 eV (10.5 or 8.0 eV on an impulsive scale). Dissociation of the singlet states of CuO^+ to form $Cu^+(^1S) + O(^1D)$ can begin at 7.42 eV (15.1 eV on an impulsive energy scale). The correspondence of these predictions with the observed behavior in Fig. 6(a) is at least plausible, and alternate explanations for this feature are not obvious.

Reactions (17) and (18) occur at very high energy and are spin-forbidden to form ground state products (Table 2). Hence, analysis of these cross sections cannot provide useful thermodynamic information. Table 3 provides optimized parameters of Eq. (2) for these cross sections as a convenient means of reproducing them. When the reaction of $Cu^+(^3D)$ is examined, however, the thresholds for these two reactions decrease drastically (Table 3). We note that formation of $Cu(^2S) + N(^4S) + NO^+(^1\Sigma^+)$ requires 3.65 eV from $Cu^+(^3D)$ excited state reactants, such that the threshold measured for $CuN + NO^+$ formation (Table 3), implies $D_0(Cu–N) = 0.5 \pm 0.3$ eV. We have little confidence in such a number, however, in part because the relative thresholds for NO^+ and CuN^+ formation have no apparent thermodynamic meaning.

4.6. Analysis of reactions with CO_2

The thermodynamic threshold for reaction (7) with $Cu^+(^1S)$ is 4.10 ± 0.12 eV (Table 4), close to the apparent threshold for this product (Fig. 3). When this cross section is analyzed using Eq. (2) and n is allowed to vary freely, the threshold obtained falls below this predicted threshold (although within the very large uncertainty). The value of n is again large, as observed in the O_2 system. Thus, we believe the observed cross section is a mixture of inefficient reaction beginning at the thermodynamic threshold and relatively efficient impulsive reactivity, which can account for the difficulty in modeling this cross section. Interestingly, the formation of $CuO^+ + C + O$ is predicted to have a threshold of 15.21 ± 0.12 eV, very close to the energy where the second feature in the CuO^+ cross section becomes obvious (Fig. 3). The relative efficiency of this process (especially considering its very high energy requirement) is

probably because formation of the separated atoms makes this reaction spin-allowed.

The apparent thresholds for CuO^+ and $CuCO^+$ formation from reaction of $Cu^+(^1S)$ with CO_2 are similar (Fig. 3). This is reasonable as $D_0(Cu^+–O) = 1.35 \pm 0.12$ eV while $D_0(Cu^+–CO) = 1.54 \pm 0.07$ eV [31]. The small size of the $CuCO^+$ cross section makes definitive analysis with Eq. (2) difficult, but the data can be reproduced using the thermodynamic threshold of 3.91 ± 0.07 eV (Table 4). There is no obvious evidence for the spin-allowed process to form $CuCO^+(^1\Sigma^+) + O(^1D)$, which should begin at 5.88 ± 0.12 eV.

When excited state Cu^+ is present in the beam, low energy features in both the CuO^+ and $CuCO^+$ cross sections appear. The thermodynamic thresholds for these spin-allowed reactions are 1.29 ± 0.12 and 1.10 ± 0.07 eV, respectively (Table 4). Analysis of these cross section features with Eq. (2) (Table 3), yields thresholds in excess of both values. The large difference in measured thresholds is inconsistent with the known thermochemistry and with the impulsive model which predicts the opposite trend. This behavior is not understood although it seems possible that it is related to impulsive behavior mixed with the same dissociation bottleneck discussed above for N_2O. As for N_2O, bond cleavage of $CO_2(^1\Sigma_g^+)$ does not form ground state products, here $CO(^1\Sigma^+) + O(^3P)$, in a spin-conserving process.

5. Conclusions

Reactions of ground ^1S and excited ^3D states of Cu^+ ions with small atmospheric molecules are reported here. Absolute cross sections for $Cu^+(^1S)$ reactions as a function of kinetic energy are determined over extended energy ranges. All reactions of ground state Cu^+ are endothermic. The O_2, CO, CO_2, NO, N_2, and N_2O systems all exhibit reactivity dominated by impulsive dynamics. Spin conservation is found to be an important effect in determining the efficiency of the reactions. Only in the NO_2 system does the endothermicity of the ground state reactions correspond to thermodynamic information. From an analysis of the kinetic energy dependence of the cross sections in this system, we determine $D_0(Cu^+–O) = 1.35 \pm 0.12$ eV, $D_0(Cu–O) = 2.94 \pm 0.12$ eV, and $IE(CuO) = 9.34 \pm 0.06$ eV, values which agree reasonably well with scant literature information. The qualitative behavior of the cross sections in the CO and NO systems indicates that CuC^+ and CuN^+ have bond energies comparable to CuO^+. In the N_2O system, we are also able to obtain $D_0(Cu^+–N_2) = 0.92 \pm 0.31$ eV from the threshold for an excited product asymptote. The N_2O system clearly shows the influence of the singlet-triplet curve crossing associated with dissociation of $N_2O(^1\Sigma^+)$ to $N_2(^1\Sigma_g^+) + O(^3P)$. The ^3D excited state of Cu^+ reacts more efficiently with these various species, such that reactions with NO, N_2O, and NO_2 become exothermic. This is particularly noteworthy when it is realized that the small features identified with ^3D reactions should probably be multiplied by a factor of 50 to put them on the correct absolute scale for reaction of pure $Cu^+(^3D)$.

We believe that a primary reason that most of the reactions studied here tend towards impulsive reactivity is that they involve the cleavage of multiple bonds. Reactions of Cu^+ with other species appear to be reasonably effective when cleavage of single covalent bonds is involved, e.g. with H_2, the alkanes, and other small molecules [2–4,6,7]. This is apparently because Cu^+ is a strong enough Lewis acid to withdraw electron density from the bonding orbitals thereby cleaving the bond. With multiple bonds, such electron withdrawal is not sufficient for efficient bond cleavage and, hence, the reactivity shifts to higher energies. In the cases of N_2O and CO_2, spin restrictions also limit the efficiency of reactions with Cu^+.

Acknowledgements

This work is supported by the National Science Foundation under grant no. 9530421. B.W. thanks the National Science Foundation for a Research Experience for Undergraduates fellowship.

References

[1] P.B. Armentrout, J.L. Beauchamp, Acc. Chem. Res. 22 (1989) 315.
[2] J.L. Elkind, P.B. Armentrout, J. Phys. Chem. 90 (1986) 6576.
[3] R. Georgiadis, E.R. Fisher, P.B. Armentrout, J. Am. Chem. Soc. 111 (1989) 4251.
[4] E.R. Fisher, P.B. Armentrout, J. Phys. Chem. 94 (1990) 1674; 98 (1994) 8260.
[5] E.R. Fisher, J.L. Elkind, D.E. Clemmer, R. Georgiadis, S.K. Loh, N. Aristov, L.S. Sunderlin, P.B. Armentrout, J. Chem. Phys. 93 (1990) 2676.
[6] D.E. Clemmer, P.B. Armentrout, J. Phys. Chem. 95 (1991) 3084.
[7] B.L. Kickel, P.B. Armentrout, J. Phys. Chem. 99 (1995) 2024.
[8] K. Seemeyer, D. Schröder, M. Kempf, L. Lettau, J. Müller, H. Schwarz, Organometallics 14 (1995) 4465.
[9] D.K. MacMillan, M.L. Gross, C. Schulze, H. Schwarz, Organometallics 11 (1992) 2079.
[10] R.B. Cody, R.C. Burnier, W.D. Reents Jr., T.J. Carlin, D.A. McCrery, R.K. Lengel, B.S. Freiser, Int. J. Mass Spectrom. Ion Phys. 33 (1980) 37.
[11] R.C. Burnier, G.D. Byrd, B.S. Freiser, Anal. Chem. 52 (1980) 1641.
[12] R.W. Jones, R.H. Staley, J. Am. Chem. Soc. 102 (1980) 3794.
[13] R.W. Jones, R.H. Staley, J. Phys. Chem. 86 (1982) 1669.
[14] C.J. Cassady, B.S. Freiser, J. Am. Chem. Soc. 107 (1985) 1566.
[15] C.B. Lebrilla, T. Drewello, H. Schwarz, Organometallics 6 (1987) 2450.
[16] K. Eller, H. Schwarz, Chem. Ber. 123 (1990) 201.
[17] K. Eller, S. Akkok, H. Schwarz, Helv. Chim. Acta 74 (1991) 1609.
[18] K. Eller, H. Schwarz, Int. J. Mass Spectrom. Ion Processes 87 (1991) 108.
[19] K. Eller, S. Karrass, H. Schwarz, Organometallics 11 (1992) 1637.
[20] K. Eller, D. Schröder, H. Schwarz, J. Am. Chem. Soc. 114 (1992) 6173.
[21] R. Wesendrup, C.A. Schalley, D. Schröder, H. Schwarz, Chem. Eur. J. 9 (1995) 608.
[22] C.A. Schalley, D. Schröder, H. Schwarz, Organometallics 14 (1995) 317.
[23] R.C. Burnier, T.J. Carlin, W.D. Reents Jr., R.B. Cody, R.K. Lengel, B.S. Freiser, J. Am. Chem. Soc. 101 (1979) 7128.
[24] P.M. Holland, A.W. Castleman Jr., J. Am. Chem. Soc. 102 (1980) 6174.
[25] R.W. Jones, R.H. Staley, J. Am. Chem. Soc. 104 (1982) 2296.
[26] P.M. Holland, A.W. Castleman Jr., J. Chem. Phys. 76 (1982) 4195.
[27] T.F. Magnera, D.E. David, D. Stulik, R.G. Orth, H.T. Jonkman, J. Michl, J. Am. Chem. Soc. 111 (1989) 5036.
[28] T.F. Magnera, D.E. David, J. Michl, J. Am. Chem. Soc. 111 (1989) 4100.
[29] P.B. Armentrout, Acc. Chem. Res. 28 (1995) 430.
[30] N.F. Dalleska, K. Honma, L.S. Sunderlin, P.B. Armentrout, J. Am. Chem. Soc. 116 (1994) 3519.
[31] F. Meyer, F.A. Khan, P.B. Armentrout, J. Am. Chem. Soc. 117 (1995) 9740.
[32] M.R. Sievers, L.M. Jarvis, P.B. Armentrout, J. Am. Chem. Soc. 120 (1998) 1891.
[33] D. Walter, P.B. Armentrout, J. Am. Chem. Soc. 120 (1998) 3176.
[34] M.M. Kappes, R.H. Staley, J. Phys. Chem. 85 (1981) 942.
[35] R.F. Porter, R.C. Schoonmaker, C.C. Addison, Proc. Chem. Soc. (1959) 11.
[36] D. Sülzle, H. Schwarz, K.H. Moock, J.K. Terlouw, Int. J. Mass Spectrom. Ion Processes 108 (1991) 269.
[37] F. Meyer, Y. Chen, P.B. Armentrout, J. Am. Chem. Soc. 117 (1995) 4071.
[38] C.E. Moore, Atomic Energy Levels, Natl. Stand. Ref. Data Ser., Natl. Bur. Stand. (NSRDS-NBS) 35 (1971)
[39] K.M. Ervin, P.B. Armentrout, J. Chem. Phys. 83 (1985) 166.
[40] R.H. Schultz, P.B. Armentrout, Int. J. Mass Spectrom. Ion Processes 107 (1991) 29.
[41] E. Teloy, D. Gerlich, Chem. Phys. 4 (1974) 417; D. Gerlich, Diplomarbeit, University of Freiburg, Federal Republic of Germany, 1971; D. Gerlich, Adv. Chem. Phys. 82 (1992) 1.
[42] B.L. Kickel, P.B. Armentrout, J. Am. Chem. Soc. 117 (1995) 4057.
[43] Vibrational frequencies (in cm^{-1}) for the reactant neutrals are 1580.19 for O_2, 2169.52 for CO, 1384.86, 667.30 (2), and 2349.30 for CO_2, 3651.1, 1594.7, and 3755.9 for H_2O, 2344.24 for N_2, and 1903.60 for NO, 1276.5, 589.2 (2), and 2223.7 for N_2O as given in reference [44].
[44] M.W. Chase, C.A. Davies, J.R. Downey, D.J. Frurip, R.A. McDonald, A.N. Syverud, J. Phys. Chem. Ref. Data 14 (1985), suppl. 1 (JANAF Tables).
[45] M.E. Weber, J.L. Elkind, P.B. Armentrout, J. Phys. Chem. 84 (1986) 1521.
[46] D.E. Clemmer, J.L. Elkind, N. Aristov, P.B. Armentrout, J. Chem. Phys. 95 (1991) 3387.
[47] M.R. Sievers, Y.-M. Chen, P.B. Armentrout, J. Chem. Phys. 105 (1996) 6322.
[48] S.G. Lias, J.E. Bartmess, J.F. Liebman, J.L. Holmes, R.D. Levin, W.G. Mallard, J. Chem. Phys. Ref. Data 17 (1988), suppl. 1.
[49] G. Gioumousis, D.P. Stevenson, J. Chem. Phys. 29 (1958) 294.
[50] L.A. Barnes, M. Rosi, C.W. Bauschlicher Jr., J. Chem. Phys. 93 (1990) 609.
[51] A.J. Merer, Annu. Rev. Phys. Chem. 40 (1989) 407.
[52] A.F. Fiedler, D. Schröder, S. Shaik, H. Schwarz, J. Am. Chem. Soc. 116 (1994) 10 734.
[53] D. Hippe, S.D. Peyerimhoff, Mol. Phys. 76 (1992) 293.
[54] D.E. Clemmer, N.F. Dalleska, P.B. Armentrout, J. Chem. Phys. 95 (1991) 7263.
[55] J.B. Pedley, E.M. Marshall, J. Phys. Chem. Ref. Data 12 (1983) 967.
[56] S. Smoes, F. Mandy, A. Vander Auwera-Mahieu, J. Drowart, Bull. Soc. Chim. Belg. 81 (1972) 45.
[57] L.R. Watson, T.L. Thiem, R.A. Dressler, R.H. Salter, E. Murad, J. Phys. Chem. 97 (1993) 5577.
[58] C. Vinckler, T. Verhaeghe, I. Vanhees, J. Chem. Soc. Faraday Trans. 90 (1994) 2003.

[59] S.R. Langhoff, C.W. Bauschlicher Jr., Chem. Phys. Lett. 124 (1986) 241.
[60] P.B. Armentrout, L.F. Halle, J.L. Beauchamp, J. Chem. Phys. 76 (1982) 2449.
[61] F.A. Khan, D.L. Steele, P.B. Armentrout, J. Phys. Chem. 99 (1995) 7819.
[62] B.L. Tjelta, P.B. Armentrout, J. Phys. Chem. 101 (1997) 2064.